Thermodynamics-Based Computational Design of Al-Mg-Sc-Zr Alloys

G.N. HAIDEMENOPOULOS, A.I. KATSAMAS, and H. KAMOUTSI

Alloying additions of Sc and Zr raise the yield strength of Al-Mg alloys significantly. We have studied the effects of Sc and Zr on the grain refinement and recrystallization resistance of Al-Mg alloys with the aid of computational alloy thermodynamics. The grain refinement potential has been assessed by Scheil–Gulliver simulations of solidification paths, while the recrystallization resistance (Zener drag) has been assessed by calculation of the precipitation driving forces of the Al_3Sc and Al_3Zr intermetallics. Microstructural performance indices have been derived, used to rank several alloy composition variants, and finally select the variant with the best combination of grain refinement and recrystallization resistance. The method can be used, with certain limitations, for a thermodynamics-based design of Al-Mg and other alloy compositions.

DOI: 10.1007/s11661-009-0168-8

I. INTRODUCTION

WHILE it has been experimentally documented[1–3] that additions of Sc or combinations of Sc and Zr can raise significantly the yield strength of Al-Mg alloys, a sound thermodynamic analysis that would allow the design of these alloys is not available. This article presents a computational thermodynamics-based method for assessing the effects of combined Sc and Zr additions on the grain refinement and recrystallization resistance of Al-Mg alloys. The method can be used for the selection of the optimum alloy variants, in an effort to reduce the time and costs related to the traditional empirical alloy development methodologies.

Non-heat-treatable aluminum alloys are utilized in all of the major industrial markets for aluminum flat-rolled products. Transportation, packaging, and the building/construction sectors represent the largest usage of non-heat-treatable sheet. Among them, wrought non-heat-treatable Al-Mg alloys are used, rather widely, as a structural material due to their good weldability, excellent corrosion resistance, and ductility. Recently there has been an increasing interest in Al-Mg alloys in the form of hot-rolled thick plates (8 to 15 mm) for marine applications. However, even alloys containing 5 to 6 pct Mg do not show adequate strength. These alloys are strengthened mainly by solid-solution strengthening from the Mg atoms and work-hardening during cold rolling. However, in hot-rolled products in which the work-hardening contribution is negligible, additional alloying is needed in order to improve the mechanical strength of the alloys.

As already mentioned, there has been sound experimental evidence that Sc and Zr additions raise the yield strength of Al-Mg alloys. The strengthening mechanisms have been discussed[4,5] and it is clear that the strength improvements obtained are mainly due to the following: (1) grain refinement of the as-cast structure (modification effect)[2] and (2) inhibition of recrystallization during hot working.[6] Precipitation strengthening[4] has also been considered; however, its contribution is not as strong as the previous two mechanisms. All these effects are activated by the formation of fine dispersions of Al_3Sc (in the case of alloying with Sc) and Al_3Sc/Al_3Zr or $Al_3(Sc_xZr_{1-x})$ (in the case of alloying with Sc and Zr) intermetallics. In the Al-Mg-Sc-Zr system under consideration, it has been found that the Al_3Sc phase dissolves approximately 12 at. pct Zr, which corresponds to the substitution of almost 50 pct of the Sc lattice sites.[7]

The grain-refining effect of Sc is attributed to the formation of primary Al_3Sc during solidification. The reason for this effect is that the Al_3Sc intermetallic, having a $L1_2$ structure with a lattice parameter of 0.4104 nm, very close to the lattice parameter of the Al-rich solid-solution matrix ($\alpha = 0.404$ nm), can act as a heterogeneous nucleation site for the matrix Al-rich phase.[5] In Al-Sc alloys, the formation of Al_3Sc takes place at Sc contents higher than 0.6 mass pct, which is higher than the eutectic composition. Similar conditions hold for the combined Sc/Zr alloying, with the additional argument that Al_3Zr precipitation occurs first from the melt and is then followed by Al_3Sc precipitation on the Al_3Zr particles. It is the combined Al_3Sc/Al_3Zr particles that have the necessary critical size to act as nucleation sites for the solidification of the matrix phase.[2]

G.N. HAIDEMENOPOULOS, Professor, and H. KAMOUTSI, Research Associate, are with the Laboratory of Materials, Department of Mechanical Engineering, University of Thessaly, Volos, Greece. Contact e-mail: hgreg@mie.uth.gr A.I. KATSAMAS, formerly Research Associate, Laboratory of Materials, Department of Mechanical Engineering, University of Thessaly, is with the Directorate of Environment and Land Planning, Region of Thessaly, Larissa, Greece.

Manuscript submitted October 1, 2009.
Article published online February 5, 2010

The recrystallization resistance is attributed to the formation of a dense distribution of Al_3Sc/Al_3Zr particles during homogenization or hot rolling in the temperature range 723 K (450 °C) to 823 K (550 °C).[5] The main effect is a strong Zener drag exerted by the particles due to the fact that they are coherent with the matrix and are very stable thermally against loss of coherency and coarsening.[5,8] Substantial improvements in recrystallization resistance have been reported.[9–11]

It has been shown that additions of Zr in Al-Sc alloys enhance the effects of Sc. The required Sc content for the formation of primary Al_3Sc during solidification decreases.[12] In addition, the coarsening resistance of the Al_3Sc dispersion and its stability against prolonged heating at high temperatures are enhanced.[13] However, there are few experimental data on the effects of combined additions of Sc and Zr in Al-Mg alloys and, more important, a thorough thermodynamic analysis of the alloy additions is missing, making the development of such alloys difficult.

The present article presents a thermodynamics-based analysis of the effects of Sc and Zr additions in the Al-Mg system, in an effort to reduce the time and costs related to the traditional empirical alloy development methodologies. At first, the alloy design requirements and the relevant mechanisms will be discussed. The computational method, including the necessary thermodynamic calculations, will be discussed in Section III. The results include three sections: a section on the calculation of precipitation driving forces (ΔG_p) that allow the base alloy matrix composition and alloy variants to be selected, a section on the Scheil solidification calculations for the as-cast microstructure refinement, and finally a section on the thermodynamic calculations for recrystallization resistance.

II. ALLOY DESIGN REQUIREMENTS

In the Al-Mg-Sc-Zr system under consideration, the design requirements, relevant mechanisms, and necessary thermodynamic calculations are summarized in Table I. The alloy is considered to be composed of the matrix and two dispersions, the grain-refining dispersion and the dispersion for the increase in the recrystallization and grain growth resistance.

A. *Matrix*

The Al_3Mg_2 phase (β phase) does not contribute significantly to strength. At the same time, the presence of the β phase degrades the corrosion resistance of Al-Mg alloys. Therefore, for solid-solution strengthening and corrosion resistance, the amount of Mg in the solid solution of the matrix α phase should be maximized and the precipitation of the β phase should be minimized. The necessary thermodynamic calculations will aim to minimize the precipitation driving force of the β phase.

B. *Grain Refinement*

For Sc and Zr additions to be efficient grain refiners, the primary Al_3Sc and Al_3Zr phases should form in the melt before the formation of the matrix α phase. As discussed earlier, the Al_3Sc particles have a lattice parameter close to that of the α phase, so that the primary Al_3Sc particles can be very effective heterogeneous nucleation sites. For the binary Al-Sc alloys, effective grain refining is exhibited for Sc contents above the eutectic composition (approximately 0.6 wt pct). However, for ternary or higher-order systems, the eutectic composition depends on the other alloying elements. For example, it has been shown that the eutectic composition of Sc decreases with increasing Mg in the alloy.[14] In addition, it has been observed that the potential of Sc as a grain refiner is increased when added together with Zr.[15] It is clear that in the Al-Mg-Sc-Zr system under consideration, the effects of combined Sc and Zr additions should be determined. The grain-refining potential will be assessed by Scheil–Gulliver simulations in order to determine the solidification path as a function of the Sc or Zr content. The aim here is to select alloy variants that maximize the mole fraction f_{bsa} of the Al_3Sc and Al_3Zr phases that form before the solidification of the α phase.

The microsegregation of alloying elements is also calculated, in order to determine the leftover Sc and Zr in the matrix, which would be available for precipitation of the secondary dispersion of Al_3Sc and Al_3Zr during homogenization or hot rolling for recrystallization resistance.

C. *Recrystallization and Grain Growth Resistance*

The small second-phase particles that form during homogenization or hot rolling (here called secondary

Table I. Alloy Design Requirements, Mechanisms, and Required Thermodynamic Calculations

Steps in Alloy Design Process	Matrix	Dispersion for Grain Refining	Dispersion for Recrystallization Resistance
Design requirements	solid solution strengthening, corrosion resistance	nucleation sites for solidification	precipitation of Al_3Sc/Al_3Zr intermetallics during hot rolling
Mechanisms	increase Mg in solid solution of α phase, minimize amount of β-Al_3Mg_2 phase	formation of Al_3Sc/Al_3Zr intermetallics before the solidification of α phase	maximize Zener drag effect (maximize f/r)
Thermodynamic calculations	minimize driving force for precipitation of β- Al_3Mg_2 phase	Scheil–Gulliver simulations for solidification paths and microsegregation	maximize the driving force for precipitation of Al_3Sc/Al_3Zr intermetallics

particles, in order to differentiate them from the primary phases) exert a restraining force on moving grain boundaries during recrystallization and grain growth. The restraining pressure p_z, which is called Zener drag,[16] is expressed by

$$p_z = \frac{3\gamma_{GB} f}{2r} \quad [1]$$

where γ_{GB} is the grain boundary energy, f the volume fraction of the particles, and r the particle radius. For a strong Zener drag effect, the ratio f/r should be maximized. The Al_3Sc and Al_3Zr secondary particles form by diffusional nucleation and growth during the homogenization or hot-rolling process. The critical nucleus size r^* for precipitation is[17]

$$r^* = -\frac{2\gamma}{\Delta G_p} \quad [2]$$

where γ is the particle/matrix interfacial energy and ΔG_p is the thermodynamic driving force for precipitation (nucleation) per unit volume. An increase in the precipitation driving force leads to refinement of the nucleus size. Furthermore, in order to inhibit significant growth and coarsening of the dispersion, a fast nucleation rate is sought, so that a significant part of the dispersion volume fraction forms during nucleation, thus maintaining a low mean particle size. The nucleation rate I may be expressed,[17] in nuclei per unit volume, by

$$I = N_o Z \beta^* \exp\left(-\frac{\Delta G^*}{kT}\right) \quad [3]$$

where N_o is the initial density of nucleation sites, Z is the Zeldovich factor, β^* is the rate of attachment of atoms to the nucleus, k is the Boltzmann constant, T is the temperature, and ΔG^* is the activation energy for nucleation, which is given by

$$\Delta G^* = \frac{16\pi\gamma^3}{3(\Delta G_p + \Delta G_\varepsilon)^2} \quad [4]$$

where ΔG_ε is the strain energy due to coherency or misfit strains between the particle and the matrix. From Eqs. [3] and [4], one concludes that an increase in the precipitation driving force ΔG_p leads to an increase in the nucleation rate and, thus, to further size refinement. From Eq. [1], the Zener drag depends on the f/r ratio. To a first approximation, one can scale r with the critical size for nucleation r^*. The ratio f/r then scales directly with the product $f\Delta G_p$.

The precipitation driving force is a thermodynamic quantity and can be calculated as a function of the temperature and alloy composition. Therefore, alloy compositions can be selected in order to maximize the product $f\Delta G_p$, a procedure that will be presented in Sections III and IV. An additional requirement for the dispersion, aiming at recrystallization and grain growth resistance, is that the particles should have a high thermodynamic stability at the submicron level in order to resist dissolution and coarsening at the high hot-rolling temperatures.

III. COMPUTATIONAL METHOD

All necessary thermodynamic calculations were performed with Thermo-Calc software (Thermocalc Software, Stockholm, Sweden)[18] which is based on the CALPHAD approach[19] for the description of the Gibbs free energy of the various phases in the system. For the Al-Mg-Sc-Zr system under consideration, appropriate thermodynamic data are necessary. One of the most comprehensive thermodynamic databases for aluminum alloys, and in general for light, nonferrous alloys, is the COST 507 database (Thermocalc Software, Stockholm, Sweden).[20] The COST 507 database contains thermodynamic data for the 19 elements most commonly encountered in Al alloys (Al, B, C, Ce, Cr, Cu, Fe, Li, Mg, Mn, N, Nd, Ni, Si, Sn, B, Y, Zn, and Zr). The element Sc is not included in the database and, therefore, it was necessary to incorporate the mathematical description of the Gibbs free energy for each phase that may form in the Al-Sc system, including solid-solution and intermetallic phases. In the binary Al–Sc system, four intermetallic phases may form, namely Al_3Sc, Al_2Sc, AlSc, and $AlSc_2$. The thermodynamic data of Sc were retrieved from the open literature and incorporated into the COST 507 database. The procedure is described in the Appendix. All calculations in the present article were performed by using the modified COST 507 + Sc database.

For a binary system A-B, with two phases α and β, the chemical driving force for precipitation of a β phase from a supersaturated solid solution of α phase can be obtained by the graphical parallel tangent construction to the two phases in the Gibbs free energy diagram of the binary system,[21] as shown in Figure 1. The precipitation driving force ΔG_m^β of the β phase is

$$\Delta G_m^\beta = -\left(X_A^\beta \mu_A^\alpha + X_B^\beta \mu_B^\alpha - G_m^\beta\right) \quad [5]$$

where X_A^β and X_B^β are the mole fractions of A and B, respectively, in the β phase, μ_A^α and μ_B^α are the chemical potentials of A and B, respectively, in the α phase, and G_m^β is the molar free energy of the β phase. The driving

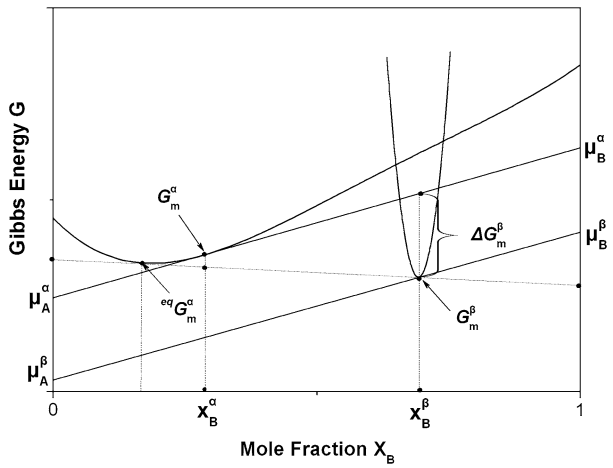

Fig. 1—Parallel tangent construction for the determination of the precipitation driving force.

force for precipitation per unit volume ΔG_p of Eqs. [2] and [4] is related to ΔG_m through the expression:

$$\Delta G_p = \frac{\Delta G_m}{V_m} \quad [6]$$

where V_m is the molar volume. Therefore ΔG_p scales directly with ΔG_m.

In the Thermo-Calc software, the equilibrium between phases is calculated by employing a "global" free energy minimization procedure. In this procedure, all phases are potential candidates to form at equilibrium and, therefore, all take part in the calculation. In Thermo-Calc, their status is characterized as "entered." However, when a phase takes part in equilibrium, the driving force for precipitation becomes zero. In order to calculate the driving force for the precipitation ΔG_m of that phase, the phase status should be characterized as "dormant." In this way, the phase does not take part in equilibrium and its driving force is calculated. This procedure has been used for the calculation of the precipitation driving forces of the β phase as well as the Al_3Sc and Al_3Zr intermetallic phases.

In order to determine the solidification paths and microsegregation, Scheil–Gulliver simulations were performed by employing the relevant module incorporated in the Thermo-Calc software. In the Scheil–Gulliver solidification model, the liquid phase is assumed to remain chemically homogeneous at all times during solidification, which implies that diffusion is considered to be infinitely fast in the liquid phase. In contrast, no diffusion at all is assumed to take place within the solid phases involved, which causes the gradual formation of concentration gradients inside the solid phases as solidification proceeds (microsegregation). Due to these basic assumptions, the Scheil–Gulliver solidification model manages to describe the solidification path of an alloy more realistically, compared to solidification under thermodynamic equilibrium conditions.

Further assumptions in the thermodynamic calculations were the following: (1) that the system under consideration was the Al-Mg-Sc-Zr-Mn-Cr and (2) that because the ternary intermetallic phase $Al_3(Sc_xZr_{1-x})$ has not been thermodynamically modeled yet, it was considered that the binary phases Al_3Sc and Al_3Zr form individually in the system.

IV. RESULTS AND DISCUSSION

A. *Calculation of Precipitation Driving Forces*

The precipitation driving forces ΔG_m for the intermetallic Al_3Sc, Al_3Zr, and β phases from the α phase (matrix Al-rich phase) have been calculated by employing the procedure described earlier. Figure 2(a) shows the ΔG_m for Al_3Sc as a function of the temperature and the Sc mass pct in the Al-5Mg-0.1Zr-Sc alloy. There is a linear increase in ΔG_m with decreasing temperature. The driving force also increases with increasing Sc content in the alloy. This variation is shown in Figure 2(b) for Al-5Mg-0.1Zr at 773 K (500 °C). The effect of the Mg content of the alloy on the ΔG_m for Al_3Sc is shown in Figure 3(a) for the Al-Mg-0.1Zr-0.4Sc alloy. The variation in the driving force with the Mg content at 773 K (500 °C) is shown in Figure 3(b).

For alloy design purposes, it is more convenient to plot iso-ΔG_m contours in the temperature-composition space, something like a driving force map. Two such maps are shown, in Figure 4(a) for the Al_3Sc in Al-5Mg-0.1Zr-Sc alloy and in Figure 4(b) for the Al_3Zr in Al-5Mg-0.1Sc-Zr alloy. The usefulness of these maps is evident in Figure 5, which depicts iso-ΔG_m contours for the β, Al_3Sc, and Al_3Zr phases in a temperature–Mg-composition diagram. From the preceding discussion on alloy design requirements, it follows that the Mg content of the alloy should be such that the driving force of the β phase is minimized while at the same time providing for a large driving force of the intermetallic phases Al_3Sc and Al_3Zr. To aid in the Mg selection, the driving force map of Figure 5 is used. Above the $\Delta G_m^{\beta} = 0$ line, there is no precipitation of the β phase, and all magnesium is in solution in the matrix α phase and increases the driving force for the precipitation of

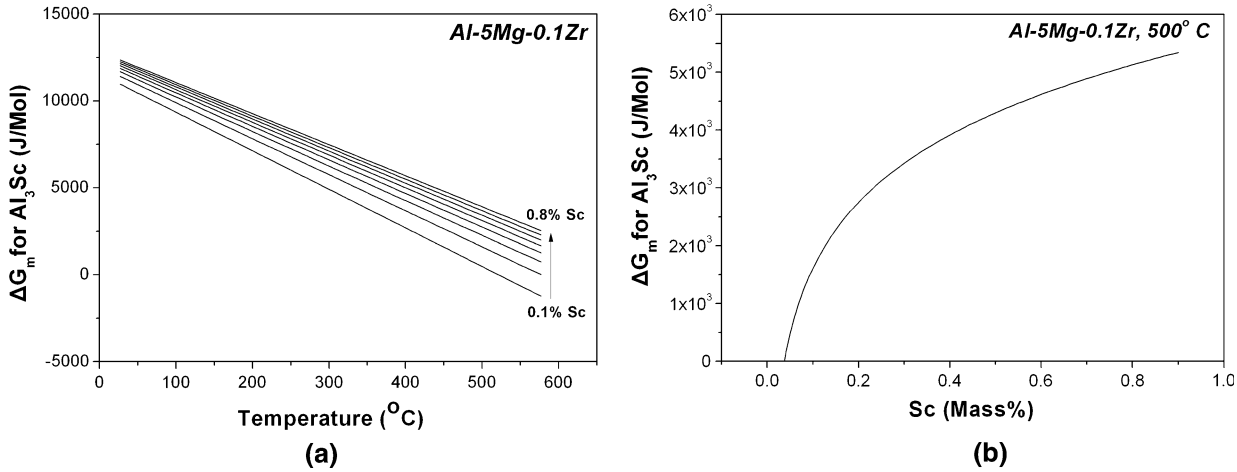

Fig. 2—Precipitation driving force of Al_3Sc: (*a*) as a function of temperature and mass pct Sc and (*b*) as a function of mass pct Sc at 773 K (500 °C).

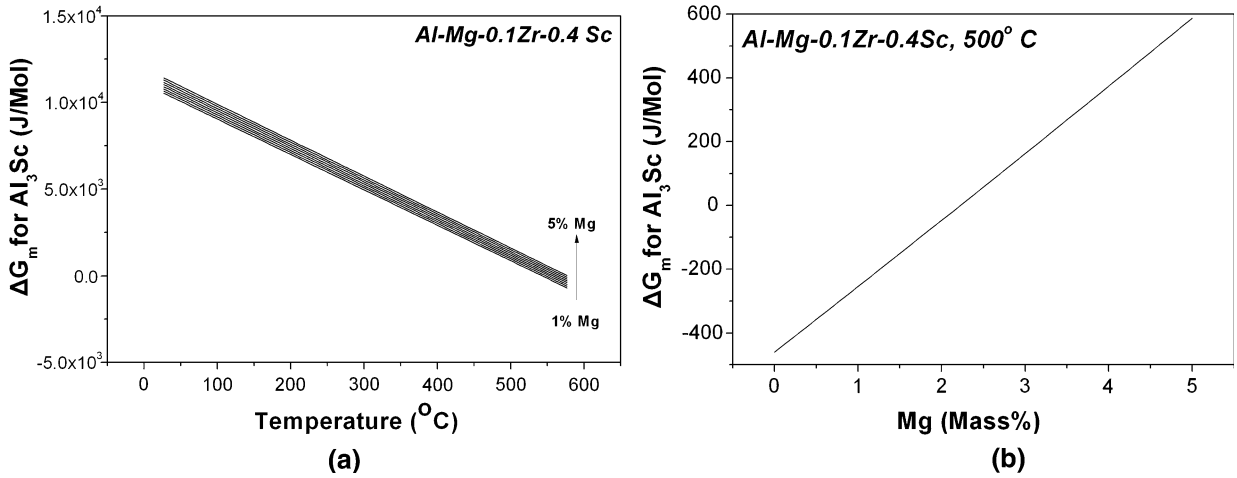

Fig. 3—Precipitation driving force of Al_3Sc: (*a*) as a function of temperature and mass pct Mg and (*b*) as a function of mass pct Mg at 773 K (500 °C).

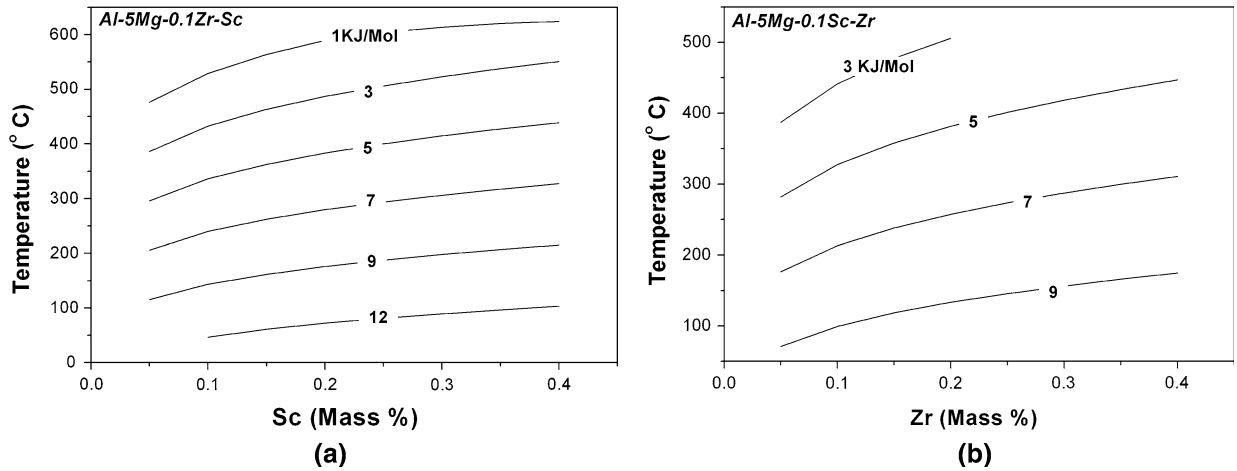

Fig. 4—Precipitation driving force contours (iso-ΔG_m curves) in temperature-composition space for: (*a*) for Al_3Sc in Al-5Mg-0.1Zr alloy and (*b*) Al_3Zr in Al-5Mg-0.1Sc alloy.

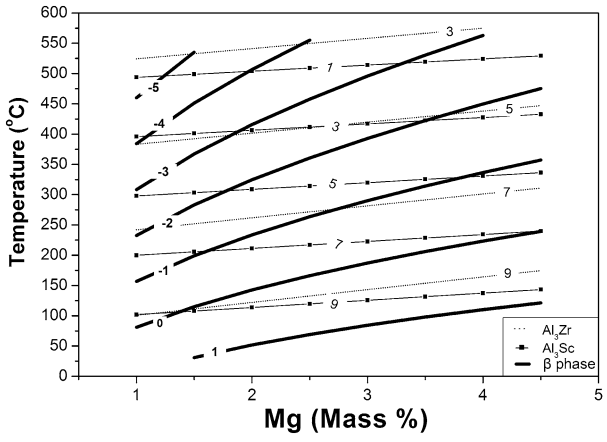

Fig. 5—Precipitation driving force contours for β phase, Al_3Sc, and Al_3Zr in temperature-mass pct Mg space for Al-Mg-0.1Sc-0.1Zr alloy. Numbers are in kJ/mol.

Table II. Alloy Variants Examined with Corresponding Sc and Zr additions (Base = Al-4.5Mg-0.55Mn-0.1Si -0.1Cr Mass Percent)

Alloy Variant	Sc (Mass Pct)	Zr (Mass Pct)
Base + 0.10Sc + 0.08Zr	0.10	0.08
Base + 0.10Sc + 0.15Zr	0.10	0.15
Base + 0.40Sc + 0.08Zr	0.40	0.08
Base + 0.40Sc + 0.15Zr	0.40	0.15

Al_3Sc and Al_3Sc. A Mg composition in the range of 4 to 5 mass pct satisfies both requirements, *i.e.*, minimal β-phase precipitation and a high driving force for Al_3Sc and Al_3Zr precipitation. This driving force is in the range 0.5 to 2.0 kJ/mol for Al_3Sc and 2 to 4 kJ/mol for Al_3Zr in the temperature range of homogenization and hot rolling (723 K (450 °C) to 823 K (550 °C)) in which

recrystallization resistance is required. Of course, these values will be altered after the precipitation of primary Al_3Sc and Al_3Zr during solidification changes the composition of the matrix α phase, an issue to be dealt later in the article. Taking this into consideration, a magnesium content of 4.5 mass pct was selected as the base alloy composition. This composition corresponds to the 5083 composition of the 5xxx series of Al alloys. In order to analyze the effects of the Sc and Zr additions, four alloy variants were selected and are shown together with the base alloy composition in Table II. These variants correspond to two levels for Sc (0.1 and 0.4 mass pct) and two levels for Zr (0.08 and 0.15 mass pct).

B. *Calculations for Grain Refinement*

As already discussed, the grain refinement of the as-cast microstructure of the alloys is one of the design requirements of this study. The main objective of this part of the work was to determine the optimum combinations of Sc and Zr additions that lead to the formation of primary Al_3Sc and Al_3Zr particles from the melt prior to the solidification of the matrix α phase. Early formation of primary Al_3Sc and Al_3Zr is desirable in this case, because the particles of these phases are expected to act as effective heterogeneous nucleation sites for the solidification of the matrix α phase, leading to grain refinement.

Scheil–Gulliver solidification simulations were performed for the base alloy and the Sc/Zr-alloy variants of Table II. Figure 6 depicts the "solidification path" of the base alloy in a temperature-*vs*-fraction solid diagram. Solidification starts at 912 K (639 °C) (liquidus temperature) with the formation of the $Al_{13}Cr_2$ intermetallic phase, which completes its solidification at 910.5 K (637.5 °C), representing a negligible fraction of the final as-cast microstructure (0.008 mass pct). The α phase starts to solidify at 910.5 K (637.5 °C) and carries on until solidification of the melt is completed (720.3 K (447.3 °C) = solidus temperature). It is interesting to note that the next phase beginning to form is the Al_6Mn intermetallic at 904 K (631 °C). By that point, a significant amount (≈30 mass pct) of the α phase has already solidified, without the aid of any heterogeneous nucleation sites.

An addition of 0.10 mass pct Sc and 0.08 mass pct Zr to the base alloy changes the solidification path, as shown in Figure 7. The liquidus temperature of the new alloy increases to 961 K (688 °C), *i.e.*, ≈50 °C higher in comparison to the base alloy. The first solid phase to form in the melt is now Al_3Zr, which continues to form down to 910 K (637 °C), at which point the α phase begins to solidify. At that point, primary Al_3Zr accounts for approximately 0.50 mass pct of the alloy, which, dispersed in the melt, provides numerous heterogeneous sites for the nucleation of the α phase. It is also interesting to note that primary Al_3Sc begins to form at 877 K (604 °C), *i.e.*, after approximately 70 pct of the matrix α phase has already solidified. Thus, in this case, it seems that the effect of Zr in terms of the as-cast microstructure refinement is much more pronounced than that of Sc. At higher levels of Sc and Zr additions, the aforementioned effects become more pronounced. For example, adding 0.40 mass pct Sc and 0.15 mass pct Zr to the base alloy leads to an even wider solidification range, *i.e.*, solidification begins at 1016 K (743 °C) and completes at 720.3 K (447.3 °C). The first solid phase to form is Al_3Zr, followed by Al_3Sc, the latter starting to solidify at approximately 100 °C lower. It should be noted that, in this case, both phases begin to solidify before the matrix phase, thus providing the necessary heterogeneous nucleation sites for grain refinement.

Figure 8 summarizes the outcome of the Scheil–Gulliver solidification simulations for the Al_3Zr phase, depicting the mole pct of Al_3Zr in the as-cast microstructure as a function of temperature during solidification of the four alloy variants. The first point here is that the Sc content of the alloy does not affect the formation of Al_3Zr. As shown, curves for the same Zr content coincide regardless of the Sc content of each alloy. The second point is that higher Zr contents lead to the earlier formation of Al_3Zr and to higher amounts of this phase

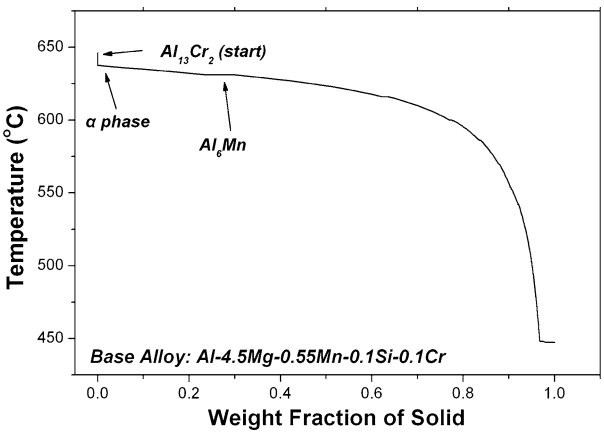

Fig. 6—Calculated solidification path of the base alloy, using the Scheil–Gulliver solidification model and Thermo-Calc software. Arrows point at the start of formation of the respective phase.

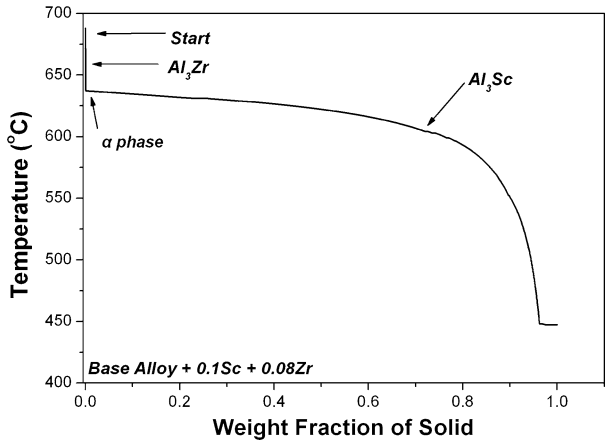

Fig. 7—Calculated solidification path of the alloy variant containing 0.10 pct Sc and 0.08 pct Zr, using the Scheil–Gulliver solidification model and Thermo-Calc software. Arrows point at the start of formation of the respective phase.

in the as-cast microstructure. The vertical dashed line in Figure 8 indicates the temperature at which the matrix α phase begins to solidify. It is evident that for all alloy variants, the matrix phase begins to solidify after the Al_3Zr phase has completed its solidification. Therefore, all the primary Al_3Zr particles can in principle act as heterogeneous nucleation sites for the solidification of the matrix phase. Furthermore, the addition of higher amounts of Zr leads to the formation of higher amounts of Al_3Zr and, thus, to a more efficient grain refinement.

A similar situation is valid for the Al_3Sc phase. Figure 9 summarizes the results of the Scheil–Gulliver simulations for Al_3Sc in the as-cast microstructure of the four alloy variants. In addition, in this case, the Zr content does not affect the formation of Al_3Sc. Higher Sc contents lead to the earlier solidification of Al_3Sc and to higher amounts of this phase in the as-cast microstructure. Once again, the vertical dashed line in Figure 9 denotes the temperature at which the α phase starts to solidify. In this case, it is evident that the two phases (Al_3Sc and α phase) either solidify largely in parallel (*e.g.*, for the 0.40 mass pct Sc-containing alloys) or Al_3Sc begins to form after a substantial amount of the α phase has already solidified (*e.g.*, for the 0.10 mass pct Sc-containing alloys), in contrast to the case for Al_3Zr discussed previously. This means that only a fraction of the Al_3Sc particles can in principle serve as heterogeneous nucleation sites for the matrix phase. In this respect, Zr is a more efficient grain refiner of the as-cast microstructure than Sc. However, the relatively high amounts of Al_3Sc forming in the 0.40 mass pct Sc-containing alloys could probably compensate for that loss of heterogeneous nucleation sites. From the preceding discussion, it seems that the mole fraction of primary phases formed before the solidification of the α phase can be used in order to quantify the grain-refining potential of the alloying elements. This point is discussed further in Section D.

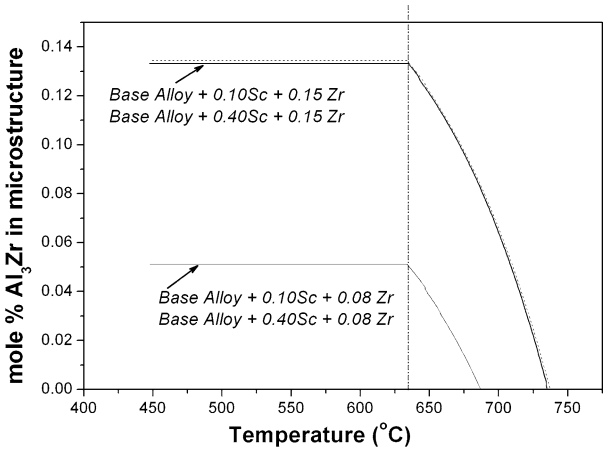

Fig. 8—Primary Al_3Zr phase in the microstructure of alloy variants during solidification. The vertical dashed line indicates the temperature at which the matrix α phase begins to solidify.

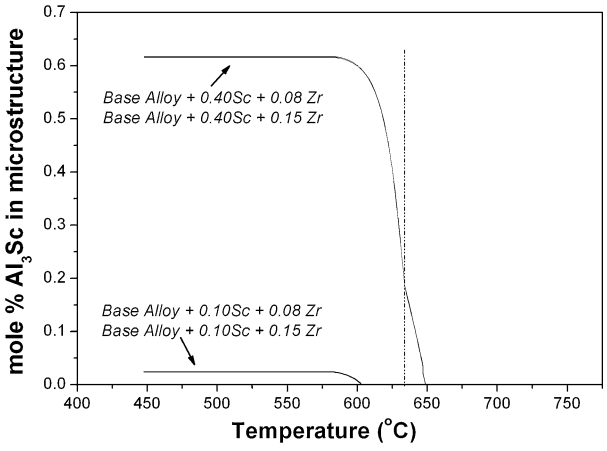

Fig. 9—Primary Al_3Sc phase in the microstructure of alloy variants during solidification. Vertical dashed line indicates the temperature at which the matrix α phase begins to solidify.

In order to calculate the precipitation driving forces of secondary Al_3Sc and Al_3Zr that form during homogenization or hot rolling, one should calculate first the Sc and Zr remaining in solution in the α phase after solidification. Therefore, the microsegregation of these elements should be calculated. Figure 10 depicts the microsegregation of Mg in the matrix α phase as mass percent Mg in the α phase as a function of the mole fraction of the solidified α phase. As shown, the first α phase to solidify contains approximately 1.50 mass pct Mg, whereas the last contains approximately 14.50 mass pct Mg. The additions of Sc and Zr in the base alloy do not affect the microsegregation of Mg in the matrix. The microsegregation of Mn is depicted in Figure 11. While the first solidified α phase contains about 0.65 mass pct Mn the last contains practically no Mn. Once again, the effect of Sc and Zr in the microsegregation of Mn seems to be negligible.

Figure 12 depicts the microsegregation of Zr in the matrix α phase. As shown, the first matrix to solidify contains approximately 0.17 mass pct Zr. However, as explained previously, primary Al_3Zr forms very early during the course of solidification. As a result, the liquid phase quickly becomes depleted of Zr and the α phase, which solidifies later, gradually dissolves smaller quantities of Zr. Practically, the last 30 pct of the matrix that solidifies contains no Zr at all in solid solution.

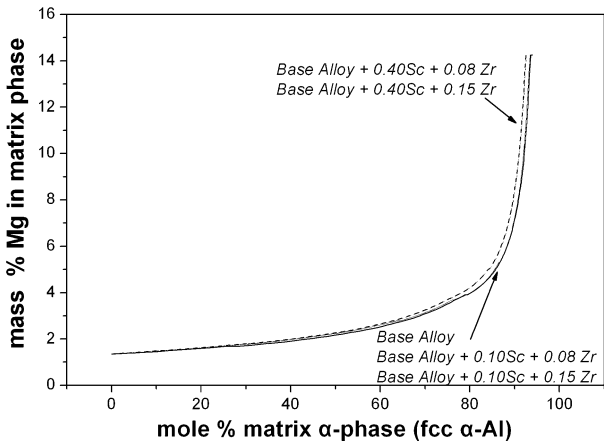

Fig. 10—Microsegregation of Mg inside the matrix phase.

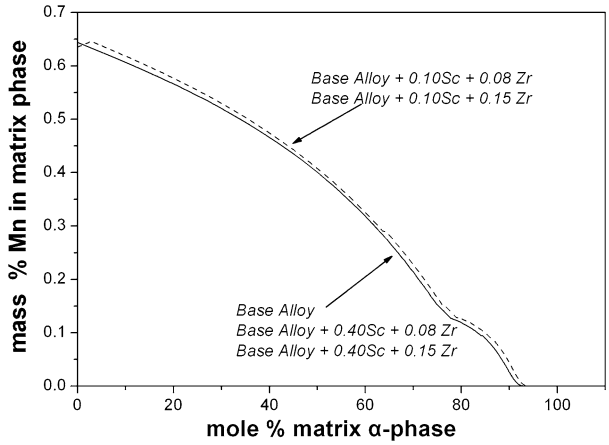

Fig. 11—Microsegregation of Mn inside the matrix phase.

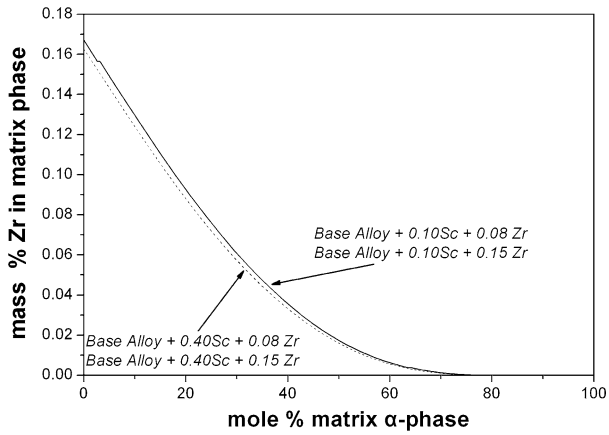

Fig. 12—Microsegregation of Zr inside the matrix phase.

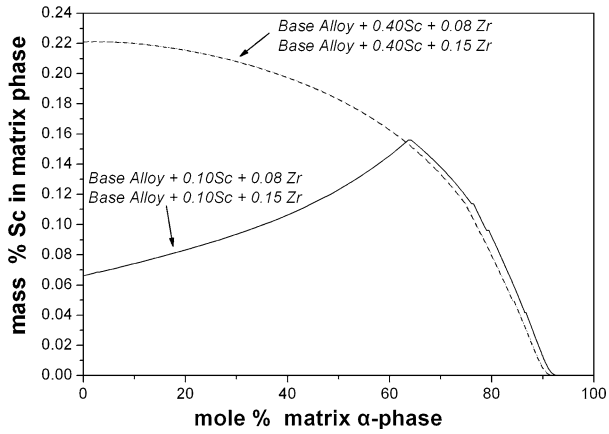

Fig. 13—Microsegregation of Sc inside the matrix phase.

The microsegregation of Sc, on the other hand, is somewhat different and depends on the Sc content of the alloy (Figure 13). The alloys containing 0.40 mass pct Sc exhibit a monotonically decreasing concentration inside the matrix phase. This happens because, as in the case of Zr, primary Al_3Sc begins to form earlier than the α phase. Thus, the liquid phase becomes gradually depleted of Sc and the subsequently solidified matrix phase contains gradually less Sc. In contrast, in the alloys containing 0.10 mass pct Sc, primary Al_3Sc begins to form after the matrix α phase. As a result, a significant fraction of the matrix phase initially incorporates increasing amounts of Sc. However, as soon as the formation of primary Al_3Sc commences, there is a reversal of this process and the concentration of Sc inside the matrix phase is decreased.

C. *Calculations for Recrystallization Resistance*

The alloy design requirements for recrystallization resistance have been discussed in Section II of this work. Recrystallization resistance is proportional to $f\Delta G_m$. The aim of this section is twofold: (1) to calculate the balance mole fractions of Al_3Zr and Al_3Sc after solidification that are available for precipitation as secondary phases at the hot-rolling temperature range and (2) to calculate the precipitation driving forces ΔG_m of secondary Al_3Sc and Al_3Zr at the hot-rolling temperature range. A temperature of 773 K (500 °C) has been selected for the calculations.

The balance mole fraction of the intermetallic phases f_{bal} is

$$f_{\text{bal}} = f_{eq} - f_{ac} \qquad [7]$$

where f_{eq} is the mole fraction of the phases at equilibrium at 773 K (500 °C) and f_{ac} is the mole fraction of the primary phases in the as-cast structure. The equilibrium mole fraction can be readily calculated by Thermo-Calc. The mole fractions f_{ac} in the as-cast structure is a value taken directly from Figures 8 and 9 for Al_3Zr and Al_3Sc, respectively. The results are given for completeness in Section D.

In order to proceed with the calculations of the precipitation driving force for the secondary Al_3Zr and Al_3Sc at 773 K (500 °C), the composition of the α phase after solidification should be determined. This composition can be derived from the microsegregation profiles of Figures 10 through 13. The profiles have been integrated in order to calculate the average compositions of the alloying elements in the α phase. This procedure gives for Zr the value of 0.052 mass pct in all four alloy variants. For Sc, the values are 0.09 mass pct for the 0.04Sc variants and 0.137 mass pct for the 0.1Sc variants. Knowing the composition of the α phase, the precipitation driving force ΔG_m of Al_3Zr and Al_3Sc at 773 K (500 °C) can be readily calculated with the procedure described in Section A. The results are presented in Section D.

D. *Alloy Design Performance Indices*

The aim of this section is to quantify the effect of alloying additions of Sc and Zr in an effort to select the alloy variant with the best combination of grain refinement and recrystallization resistance. To assess

the grain-refining potential, the grain-refining index M_{GR} is defined with

$$M_{GR} = (f_{\text{bsa}})_{\text{Al}_3\text{Zr}} + (f_{\text{bsa}})_{\text{Al}_3\text{Sc}} \quad [8]$$

where f_{bsa} denotes the mole fraction of the primary Al_3Zr and Al_3Sc formed before solidification of the α phase. The f_{bsa} values can be read directly from Figures 8 and 9. To assess the potential for recrystallization resistance, the recrystallization resistance index M_{RX} is defined with

$$M_{RX} = (f_{\text{bal}}\Delta G_m)_{\text{Al}_3\text{Zr}} + (f_{\text{bal}}\Delta G_m)_{\text{Al}_3\text{Sc}} \quad [9]$$

where f_{bal} is the balance mole fractions of Al_3Zr and Al_3Sc (secondary phases) for precipitation at 773 K (500 °C), given by Eq. [7], and ΔG_m is the driving force of Al_3Zr and Al_3Sc for precipitation at 773 K (500 °C).

Finally, for the ranking of the four alloy variants, the overall alloy performance index M is defined as

$$M = M_{GR}M_{RX} \quad [10]$$

The results, for the four alloy variants, are assembled in Table III.

The alloy variant with the highest grain-refining potential is the 0.4Sc + 0.15Zr alloy with M_{GR} = 0.296. According to the discussion in Section B, all the Al_3Zr in the as-cast structure forms before solidification of the α phase, *i.e.*, $f_{\text{bsa}} = f_{ac}$, indicating that Zr is a more potent grain-refining addition than Sc. However, the large volume fraction of Al_3Sc formed in the 0.4Sc variants provides the necessary heterogeneous nucleation sites for the solidification of the α phase. The alloy variant with the highest recrystallization resistance is the 0.4Sc + 0.08Zr, with M_{RX} = 417.51. Although the 0.1Sc variants possess a substantially higher driving force ΔG_m for the precipitation of Al_3Sc, the 0.4Sc variants possess higher mole fractions of the secondary Al_3Sc phase f_{bal}. Because recrystallization resistance depends on the product $f_{\text{bal}}\Delta G_m$, the 0.4Sc variants have a higher index. The 0.4Sc + 0.08Zr possesses a higher index because of the high f_{bal}, which is due to the lower f_{ac} value in this alloy, *i.e.*, the mole fraction of primary Al_3Zr and Al_3Sc in the as-cast structure. So far, the method results in a different alloy variant for each of the two alloy design criteria. The 0.4Sc + 0.15Zr alloy has a greater grain-refining potential and the alloy 0.4Sc + 0.08Zr has a greater potential for recrystallization resistance. The overall performance index M of Eq. [10] is used to rank the alloy variants in terms of overall performance, *i.e.*, a combination of grain refinement and recrystallization resistance. The best choice here is alloy 0.4Sc + 0.15Zr followed by 0.4Sc + 0.08Zr, 0.1Sc + 0.15Zr, and 0.1Sc + 0.08Zr.

It should be noted that in the derivation of the overall alloy performance index in Eq. [10], the two indices M_{GR} and M_{RX} were considered as independent. However, there is some interdependence, stemming from the fact that grain size refinement imparts some influence on recrystallization resistance. This means that the primary intermetallics also influence the recrystallization resistance through grain refinement. This issue will be dealt with in the continuation of this work.

E. *Concluding Remarks*

In the treatment described, both indices M_{GR} and M_{RX} are derived with the aid of computational thermodynamics. The M_{GR} is derived by Scheil–Gulliver calculations of f_{bsa}, the mole fraction of intermetallic phases formed before solidification of the matrix α phase. The M_{RX} is derived by the Scheil–Gulliver calculation of f_{bal}, the mole fraction of intermetallics available for precipitation after solidification is complete, and the precipitation driving force ΔG_m calculations at the hot-rolling temperature. Therefore, the selection of the alloy with the highest performance index among other alloy variants is completely based on computational alloy thermodynamics. The procedure outlined here exploits the predictive power of alloy thermodynamics, because it involves thermodynamics in the alloy design stage before the alloy is actually developed. In its generalized form, the method would enable the design of alloy compositions very close to the optimum composition, so that only a fraction of experimental work will be needed relative to the empirical trial-and-error methodologies for full alloy development. On the other hand, the method possesses certain limitations, the most important of which is the fact that it relies solely on thermodynamics. Kinetics, interface, and strain energy effects are not taken into account in the derivation of the various indices.

Table III. Calculation of Performance Index of Alloy Variants

	f_{ac}*		f_{bsa}		f_{eq}		f_{bal}		ΔG_m		$f_{\text{bal}}\Delta G_m$				
Alloy Variant	Al_3Zr	Al_3Sc	Al_3Zr	Al_3Sc	Al_3Zr	Al_3Sc	Al_3Zr	Al_3Sc	Al_3Zr	Al_3Sc	Al_3Zr	Al_3Sc	M_{GR}	M_{RX}	M
0.1Sc-0.08Zr	0.048	0.031	0.048	0	0.06	0.153	0.012	0.122	865	2120	10.58	258.64	0.048	269.02	12.91
0.4Sc-0.08Zr	0.051	0.591	0.051	0.16	0.06	0.877	0.009	0.286	854	1433	7.68	409.83	0.211	417.51	88.09
0.1Sc-0.15Zr	0.132	0.029	0.132	0	0.142	0.154	0.010	0.125	865	2120	8.65	265	0.132	273.65	36.12
0.4Sc-0.15Zr	0.136	0.600	0.136	0.16	0.143	0.877	0.007	0.277	854	1433	5.97	396.94	0.296	402.91	119.27

*Definitions: f_{ac} is the mole fraction of phase in as-cast microstructure, f_{bsa} is the mole fraction of phase formed during solidification before α phase, f_{eq} is the mole fraction of phase at equilibrium at 773 K (500 °C), $f_{\text{bal}} = f_{eq} - f_{ac}$ is the balance mole fraction of phase left for precipitation at 773 K (500 °C), ΔG_m is the precipitation driving force at 773 K (500 °C), $M_{GR} = (f_{\text{bsa}})_{\text{Al}_3\text{Zr}} + (f_{\text{bsa}})_{\text{Al}_3\text{Sc}}$ is the grain-refining index, $M_{RX} = (f_{\text{bal}}\Delta G_m)_{\text{Al}_3\text{Zr}} + (f_{\text{bal}}\Delta G_m)_{\text{Al}_3\text{Sc}}$ is the recrystallization resistance index, and $M = M_{GR}M_{RX}$ is the overall alloy performance index.

Implementation of these effects will certainly lead to a different set of performance indices, for a more efficient and reliable computational alloy design.

V. CONCLUSIONS

The work described in this article presented a method to quantify the effects of Sc and Zr on the grain refinement and recrystallization resistance of Al-Mg alloys. The method involved the derivation of performance indices with the aid of computational alloy thermodynamics.

The grain-refining index was derived by the calculation of the mole fraction of Al_3Sc and Al_3Zr formed before the solidification of the matrix α phase by employing Scheil–Gulliver simulations of the solidification paths of four alloy variants based on an Al-4.5Mg base alloy. The index for the recrystallization resistance was based on the Zener drag effect and was derived by the calculation of the precipitation driving forces of secondary Al_3Sc and Al_3Zr at the hot-rolling temperature.

Among the four alloy variants studied, the 0.4Sc + 0.15Zr presented the highest potential for grain refinement, while the 0.4Sc + 0.08Zr variant presented the highest potential for recrystallization resistance. However, the alloy variant 0.4Sc + 0.15Zr presented the best combination of both grain refinement and recrystallization resistance.

The method could, under certain limitations, be used for the computational design of alloy compositions in Al-Mg and other alloys.

ACKNOWLEDGMENTS

This work has been partially supported by the Greek Secretariat of Research and Technology (Athens, Greece) under Grant No. 05PAV81. The authors thank Drs. D. Skarmoutsos of ELKEME (Athens, Greece) and D. Spathis of ELVAL (Oinofyta, Greece) for helpful suggestions.

APPENDIX

Introduction of Sc in the COST 507 light-alloy thermodynamic database

The present appendix presents the procedure for the introduction of Sc in the COST 507 thermodynamic database. This was necessary in order to carry out thermodynamic calculations involving Sc as an alloying element in Al-Mg alloys with Thermo-Calc software.

Table IV. Fundamental Thermodynamic Properties of Elemental Sc

Crystal Structure	Atomic Mass	SER Enthalpy ($H^o_{298.15} - H^o_0$ (in J/mol))	SER Entropy (S_o (in J/mol·K))
hcp	44.9559	5220	34.60

The fundamental thermodynamic properties of elemental Sc, *i.e.*, a stable crystal structure, atomic mass, and standard element reference (SER) enthalpy and entropy are given in Table IV. The following descriptions of the molar Gibbs free energies of the intermetallic phases were retrieved from the literature:[22]

$$G^{Al_3Sc} = 0.75G^{\circ,fcc}_{Al} + 0.25G^{\circ,hcp}_{Sc} - 42000 + 7.1932T \quad [A1]$$

$$G^{Al_2Sc} = 0.667G^{\circ,fcc}_{Al} + 0.333G^{\circ,hcp}_{Sc} - 48000 + 7.5T \quad [A2]$$

$$G^{AlSc} = 0.50G^{\circ,fcc}_{Al} + 0.50G^{\circ,hcp}_{Sc} - 46000 + 6.9371T \quad [A3]$$

$$G^{AlSc_2} = 0.333G^{\circ,fcc}_{Al} + 0.667G^{\circ,hcp}_{Sc} - 37000 + 3.7333T \quad [A4]$$

In Eqs. [A1] through [A4], G^{φ} represents the molar Gibbs free energy of intermetallic phase φ, $G^{\circ,fcc}_{Al}(T)$ and $G^{\circ,hcp}_{Sc}(T)$ represent the Gibbs free energy of pure Al and pure Sc, respectively, at their stable crystal structure as a function of temperature, while T is the absolute temperature. The Gibbs free energies of pure Al and pure Sc as functions of temperature are given by the following equations:

1. *Al in the fcc phase*

for 298 K ≤ T ≤ 700 K (25 °C ≤ T ≤ 427 °C):

$$G^{\circ,fcc}_{Al} = -7976.15 + 137.093038T - 24.3671976T\ln(T) - 0.001884662T^2 - 8.77664 \times 10T^3 + 74092T^{-1} \quad [A5]$$

for 700 K ≤ T ≤ 933 K (427 °C ≤ T ≤ 660 °C):

$$G^{\circ,fcc}_{Al} = -11276.24 + 223.048446T - 38.5844296T\ln(T) + 0.018531982T^2 - 5.764227 \times 10^{-6}T^3 + 74092T^{-1} \quad [A6]$$

for T ≥ 933 K (T ≥ 660 °C):

$$G^{\circ,fcc}_{Al} = -11278.378 + 188.684153T - 31.748192T\ln(T) - 1.230524 \times 10^{28}T^{-9} \quad [A7]$$

2. *Sc in the hcp phase*

for 298 K ≤ T ≤ 800 K (25 °C ≤ T ≤ 527 °C):

$$G^{\circ,hcp}_{Sc} = -8689.547 + 153.48097T - 28.1882T\ln(T) + 0.00321892T^2 - 1.64531 \times 10^{-6}T^3 + 72177T^{-1} \quad [A8]$$

for 800 K ≤ T ≤ 1608 K (527 °C ≤ T ≤ 1335 °C):

$$G^{\circ,hcp}_{Sc} = -7511.295 + 132.759582T - 24.9132T\ln(T) - 5.73295 \times 10^{-4}T^2 - 8.59345 \times 10^{-7}T^3 \quad [A9]$$

for $T \geq 1608$ K ($T \geq 1335$ °C):

$$G_{Sc}^{\circ,hcp} = +261143.04 - 1817.92245T + 241.441051T\ln(T) - 0.117529396T^2 + 8.7398 \times 10^{-6}T^3 - 50607159T^{-1} \quad [A10]$$

The corresponding mathematical description of the Gibbs free energy of solid-solution phases in the CALPHAD method is implemented by the Redlich–Kister–Mugiannu formalism.[23] According to this formalism, the molar Gibbs free energy of a nonstoichiometric phase φ is given by a relation of the following form:

$$G^{\phi} = \sum_i x_i G_i^{\circ,\phi} + RT\sum_i x_i \ln x_i + \sum_i \sum_{i>j} x_i x_j \sum_u L_{i,j}^{u,\phi}(x_i - x_j)^u \quad [A11]$$

In Eq. [A11], x_i and x_j represent the mole fractions of components i and j, respectively, $G_i^{\circ,\phi}$ is the Gibbs free energy of pure component i, when existing in the crystal structure of phase φ (*e.g.*, $G_{Al}^{\circ,fcc}$, $G_{Sc}^{\circ,hcp}$, *etc.*), while $L_{i,j}^{u,\phi}$ are the interaction parameters of order u, through which the excess energy that arises from the fact that the solid-solution phase φ is not ideal is taken into account. The available interaction parameters for the Al-Sc binary system are listed here. Interaction parameters not contained in the list are taken to be equal to zero.

$$L_{Al,Sc}^{0,fcc} = -107664.4 + 8.3T \quad [A12]$$

$$L_{Al,Sc}^{0,bcc} = -106506.3 - 2.7746T \quad [A13]$$

$$L_{Al,Sc}^{1,bcc} = -19908.5 \quad [A14]$$

$$L_{Al,Sc}^{0,hcp} = -106375.1 + 15.3157T \quad [A15]$$

$$L_{Al,Sc}^{0,liquid} = -126270.4 + 17.6241T \quad [A16]$$

Finally, the relevant $G_i^{\circ,\phi}$ parameters of Eq. [A11] are given here. It should be noted that parameters $G_{Al}^{\circ,fcc}$ and $G_{Sc}^{\circ,hcp}$ have already been described in Eqs. [A5] through [A10] and are not repeated here.

$$G_{Al}^{\circ,bcc} = 10083 - 4.813T + G_{Al}^{\circ,fcc} \quad [A17]$$

$$G_{Al}^{\circ,hcp} = 5481 - 1.8T + G_{Al}^{\circ,hcp} \quad [A18]$$

3. *Al in the liquid phase*

for 298 K $\leq T \leq$ 934 K (25 °C $\leq T \leq$ 661 °C):

$$G_{Al}^{\circ,liquid} = 11005.029 - 11.841867T + 7.934 \times 10^{-20}T^7 + G_{Al}^{\circ,fcc} \quad [A19]$$

for $T \geq 934$ K ($T \geq 661$ °C):

$$G_{Al}^{\circ,liquid} = 10482.382 - 11.253974T + 1.231 \times 10^{28}T^{-9} + G_{Al}^{\circ,fcc} \quad [A20]$$

$$G_{Sc}^{\circ,fcc} = 5000 + G_{Sc}^{\circ,hcp} \quad [A21]$$

4. *Sc in the bcc phase*

for 298 K $\leq T \leq$ 1000 K (25 °C $\leq T \leq$ 727 °C):

$$G_{Sc}^{\circ,bcc} = 1979.728 - 1.024135T + G_{Sc}^{\circ,hcp} \quad [A22]$$

for 1000 K $\leq T \leq$ 1608 K (727 °C $\leq T \leq$ 1335 °C):

$$G_{Sc}^{\circ,bcc} = 230161.408 - 2004.05469T + 276.76664T\ln(T) - 0.167120107T^2 + 1.5637371 \times 10^{-5}T^3 - 33783257T^{-1} \quad [A23]$$

for $T \geq 1608$ K ($T \geq 1335$ °C):

$$G_{Sc}^{\circ,bcc} = -25928.011 + 283.642312T - 44.2249T\ln(T) \quad [A24]$$

5. *Sc in the liquid phase*

for 298 K $\leq T \leq$ 1608 K (25 °C $\leq T \leq$ 1335 °C):

$$G_{Sc}^{\circ,liquid} = 6478.66 + 45.427539T - 10.7967803T\ln(T) - 0.020636524T^2 + 2.13106 \times 10^{-6}T^3 - 158106T^{-1} \quad [A25]$$

for $T \geq 1608$ K ($T \geq 1335$ °C):

$$G_{Sc}^{\circ,liquid} = -11832.111 + 275.871695T - 44.2249T\ln(T) \quad [A26]$$

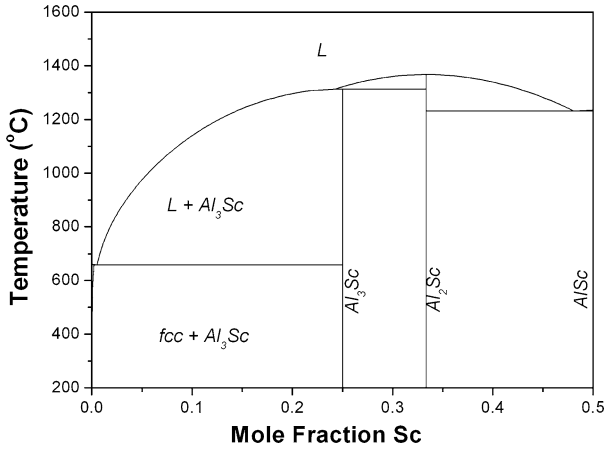

Fig. A1—Calculated binary Al-Sc phase diagram with modified COST 507 + Sc database.

After retrieving the necessary thermodynamic data for the Al-Sc system, the data were incorporated in the COST 507 database. This modified COST 507 + Sc database was then used in conjunction with Thermo-Calc software to calculate the binary Al-Sc system. The calculation was performed up to 50 at. pct Sc and is shown in Figure A1. The comparison with the published experimental binary Al-Sc[22] shows that the calculated diagram is in good agreement with the experimental one and, therefore, the modified COST 507 + Sc database can be used for the thermodynamic calculations in this work.

REFERENCES

1. V.I. Elagin, V.V. Zakharov, and T.D. Rostova: *Metalloved. Termich. Obrab. Metallov.*, 1992, vol. 1, pp. 24–28.
2. Z. Yin, Q. Pan, Y. Zhang, and F. Jiang: *Mater. Sci. Eng., A*, 2000, vol. 280, pp. 151–55.
3. Y.A. Filatov, V.I. Yelagin, and V.V. Zakharov: *Mater. Sci. Eng., A*, 2000, vol. 280, pp. 97–101.
4. K.L. Kendig and D.B. Miracle: *Acta Mater.*, 2002, vol. 50, pp. 4165–4417.
5. J. Royset and N. Ryum: *Int. Mater. Rev.*, 2005, vol. 50 (1), pp. 19–44.
6. V. Ocenasek and M. Slamova: *Mater. Charact.*, 2001, vol. 47, pp. 157–62.
7. F. Zeng, C. Xia, and Y. Gu: *J. Alloys Compd.*, 2004, vol. 363, pp. 175–81.
8. B. Forbord, H. Hallem, and K. Marthinsen: *Mater. Sci. Eng., A*, 2004, vols. 387–389, pp. 936–39.
9. Y.W. Riddle and T.H. Sanders: *Mater. Sci. Forum*, 2000, vols. 331–337, pp. 939–44.
10. J.S. Vetrano, S.M. Bruemmer, L.M. Pawloski, and I.M. Robertson: *Mater. Sci. Eng., A*, 1997, vol. 238, pp. 101–07.
11. V.I. Elagin, V.V. Zakharov, and T.D. Rostova: *Met. Sci. Heat Treat.*, 1992, vol. 1, pp. 37–45.
12. V.G. Davydov, T.D. Rostova, V.V. Zakharov, Y.A. Filatov, and V.I. Yelagin: *Mater. Sci. Eng., A*, 2000, vol. 280, pp. 30–36.
13. Y.W. Riddle, H. Hallem, and N. Ryum: *Mater. Sci. Forum*, 2002, vols. 396–402, pp. 563–68.
14. A. Pisch, J. Groebner, and R. Schmid-Fetzer: *Mater. Sci. Eng., A*, 2000, vol. 289A, pp. 123–29.
15. A.F. Norman, P.B. Pragnell, and R.S. McEwen: *Acta Mater.*, 1998, vol. 46, pp. 5715–32.
16. C. Zener: *Trans. Am. Inst. Min. Metall. Eng.*, 1946, vol. 167, pp. 551–95.
17. H.I. Aaronson and K.C. Russell: in *Solid → Solid Phase Transformations*, H.I. Aaronson, D.E. Laughlin, and C.M. Wayman, eds., TMS-AIME, Warrendale, PA, 1982, pp. 371–98.
18. B. Sundman, B. Jansson, and J.-O. Anderson: *CALPHAD*, 1985, vol. 9, pp. 153–90.
19. N. Saunders and A.P. Miodownik: *CALPHAD: Calculation of Phase Diagrams*, Pergamon, Oxford, UK, 1998, pp. 91–110.
20. G. Effenberg: COST 507: Definition of Thermochemical and Thermophysical Properties to Provide a Database for the Development of New Light Alloys. European Cooperation in the Field of Scientific and Technical Research, European Commission. Vol 1. Proceedings of the Final Workshop of COST 507, Vaals, the Netherlands, 1997. Vol 2. Thermochemical Database for Light Metal Alloys (I. Ansara, A.T. Dinsdale, and M.H. Rand, eds.). Vol 3. Critical Evaluation of Ternary Systems.
21. K. Janssens, D. Raabe, E. Kozeschnik, M.A. Miodownik, and B. Nestler: *Comput. Mater. Eng.*, Elsevier Academic Press, Burlington, MA, 2007, pp. 28–30.
22. G. Cacciamani, P. Riani, G. Borzone, N. Parodi, A. Saccone, R. Ferro, A. Pisch, and R. Schmid-Fetzer: *Intermetallics*, 1999, vol. 7, pp. 101–08.
23. O. Redlich and A.T. Kister: *Ind. Eng. Chem.*, 1948, vol. 40 (2), pp. 345–48.